Journal Pre-proof

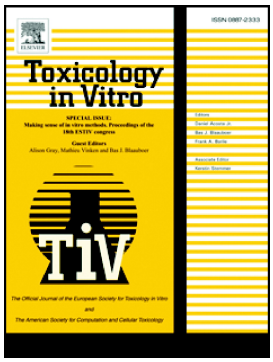

Curcumin analog, WZ37, promotes G2/M arrest and apoptosis of HNSCC cells through Akt/mTOR inhibition

Ziheng Zhang, Renyu Lin, Zhoudi Liu, Tao Yan, Yiqun Xia, Leping Zhao, Feng Lin, Xi Zhang, Chenglong Li, Yi Wang

PII: S0887-2333(19)30325-X

DOI: https://doi.org/10.1016/j.tiv.2019.104754

Reference: TIV 104754

To appear in: *Toxicology in Vitro*

Received date: 26 April 2019

Revised date: 2 December 2019

Accepted date: 17 December 2019

Please cite this article as: Z. Zhang, R. Lin, Z. Liu, et al., Curcumin analog, WZ37, promotes G2/M arrest and apoptosis of HNSCC cells through Akt/mTOR inhibition, *Toxicology in Vitro*(2019), https://doi.org/10.1016/j.tiv.2019.104754

Curcumin analog, WZ37, promotes G2/M arrest and apoptosis of HNSCC cells through Akt/mTOR inhibition

Ziheng Zhang[1,2,3,#], Renyu Lin,[1,2,#], Zhoudi Liu[1], Tao Yan[1], Yiqun Xia[2], Leping Zhao[3], Feng Lin[2], Xi Zhang[3], Chenglong Li[1], Yi Wang[1,*]

[1] Chemical Biology Research Center, School of Pharmaceutical Sciences, Wenzhou Medical University, Wenzhou, Zhejiang 325035, China

[2] The First Affiliated Hospital of Wenzhou Medical University, Wenzhou, Zhejiang 325035, China

[3] Department of Pharmacy, the Affiliated Yueqing Hospital of Wenzhou Medical University, Wenzhou, Zhejiang 325000, China

# These authors contribute equally to this work.

Running title: W37 inhibits Akt/mTOR in HNSCC

***Corresponding author:**

Yi Wang, Ph.D, Associate Professor

Address: Chemical Biology Research Center, School of Pharmaceutical Sciences, Wenzhou Medical University, Wenzhou 325035, China

Tel: +86-577-85773060; Fax: +86-577-85773060;

E-mail: yi.wang1122@wmu.edu.cn

Abbreviations

DMSO, dimethyl sulfoxide; ER, endoplasmic reticulum; HNSCC, head and neck squamous cell carcinoma; AM, acetoxymethyl; MTT, 3-(4,5-dimethyl-2-thiazolyl)-2,5-diphenyltetrazolium bromide; NAC, N-acetyl cysteine; $\Delta\psi m$, mitochondrial membrane potential; PI, propidium iodide; PVDF, polyvinylidene difluoride; ROS, reactive oxygen species; TEM, transmission electron microscopy; UPR, unfolded protein response

ABSTRACT

Head and neck squamous cell carcinoma (HNSCC) is a leading form of malignancy arising from the head and neck region. Existing conventional therapies are toxic and induce resistance to advanced HNSCC, therefore, new highly efficient therapeutic agents are urgently needed. The present study investigated the anti-cancer efficacy of WZ37, a curcumin analog, in HNSCC cell lines, and defined the mechanism of this activity. Results indicated that WZ37 inhibited proliferation of several HNSCC cell types by G2/M cycle arrest, promoted expression of a pro-apoptotic protein profile, and induced ROS-dependent mitochondrial injury and ER stress. Pre-treatment with NAC, an ROS scavenger, lowered the anti-cancer activity of WZ37 in HEP-2 cells. Long-term treatment of WZ37 (24 h) decreased Akt/mTOR phosphorylation which was accompanied by increased expression of BAD and PTEN. Moreover, co-treatment of WZ37 with MK-2206 (Akt inhibitor) promoted cancer cell apoptosis. Our findings indicated that the anti-cancer potential of WZ37 was attributed to ROS-dependent cell cycle arrest, mitochondrial injury, and ER stress, leading to apoptosis. The basis of the HNSCC cell apoptosis was through a mechanism of inhibition of the oxidant-sensitive Akt/mTOR pathway. We conclude that WZ37 can be a promising anti-cancer agent for the treatment of HNSCC.

KEYWORDS

HNSCC; curcumin analog WZ37; reactive oxygen species; calcium homeostasis; Akt/mTOR pathway

1. Introduction

Head and neck squamous cell carcinoma (HNSCC), including laryngocarcinoma and nasopharyngeal carcinoma, is a leading form of malignancy arising from the head and neck region (Rayess et al., 2018). HNSCC accounts for approximately 350,000 annual deaths globally (Rayess et al., 2018). The prognosis of HNSCC patients has improved markedly in past decades, with most being treated by surgical resection and radiotherapy for the early stage of the HNSCC (Yamazaki et al., 2017). At advanced stages, treatment may be multimodal with surgery combined with chemotherapy. Despite advances in surgery, chemotherapy, and radiotherapy, the five-year survival rate has remained essentially low (Ho et al., 2017). However, inherent and acquired resistance to the therapy limits its clinical effectiveness (Nicco and Batteux, 2017), which is reflected by poor patient survival rate. Chemoresistant cells can evade cell death signals through drug efflux, metabolic change, alteration in DNA damage repair mechanisms and/or by other unknown mechanisms (Kupsco and Schlenk, 2015). Therefore, new approaches are needed to improve the therapeutic options to decrease HNSCC incidence and severity associated with this kind of cancer.

Oxidative stress, defined as excessive amounts of cellular reactive oxygen species (ROS), is implicated in a number of diseases including cancer (Senft and Ronai, 2015). Cancer cells exhibit an higher ROS content than normal cells, developing resistance to pro-inflammatory and pro-apoptotic molecules in order to safeguard their own survival (Shpilka and Haynes, 2017). Moreover, uncontrolled high levels of ROS activate pro-apoptotic signalling pathways, particularly endoplasmic reticulum (ER) stress, mitochondrial dysfunction, ultimately leading to cellular apoptosis. The ER is a central organelle in which proteins are synthesized and properly folded. In cancer cells, these protein processing activities are particularly active under conditions of uncontrolled or impaired signalling pathways, such as the intracellular content of ROS and Ca^{2+} (Hou et al., 2017). During

protein processing (in a normal or pathological milieu), an accumulation of unfolded or misfolded proteins in the ER lumen activates the unfolded protein response (UPR), a highly conserved cellular stress response occurring in mammals as well as yeast and worm organisms (Zou et al., 2015). The UPR is a cell survival response, attempting to restore normal cell function by halting protein translation and cell cycle progression, degrading unfolded/misfolded proteins, and activating signals to promote proper protein folding (Poorghorban et al., 2015). However, if these objectives are not achieved within a certain time, the UPR activates steps for apoptosis (Leone et al., 2019). Therefore, the regulation of apoptosis and cell cycle arrest are potential key cellular pathways which can be exploited for anti-cancer mechanisms.

Curcumin is a naturally occurring hydrophobic polyphenol isolated from the rhizome of the herb *Curcuma longa*, which has a wide spectrum of pharmacological activities including anti-cancer effects by targeting a multitude of signalling pathways (Capodanno et al., 2017). To-date, three different phase-I clinical trials demonstrated that curcumin at a high dose of 12 g/day is relatively safe and well-tolerated. However, despite its biological efficacy and safety, curcumin has yet to be approved for cancer therapy due to its low bioavailability caused by poor solubility and short biological half-life. In recent years, our laboratory has focused on development of curcumin derivatives with more favorable *in vivo* bioavailability and therapeutic efficacy. We have synthesized stable mono-carbonyl analogs of curcumin by deletion of the β-diketone moiety, and one of these is WZ37, which displayed improved anti-inflammatory activity (Wang et al., 2015). The present study investigated the anti-cancer efficacy of WZ37 in HNSCC cell lines, and defined the mechanism of this activity. Our findings indicated that WZ37 induced ROS-dependent apoptosis through mitochondrial collapse, and ER stress, which was regulated by inactivation of Akt/mTOR signalling.

2. Material and methods

2.1 Chemicals and reagents

Curcumin, 3-(4,5-dimethyl-2-thiazolyl)-2,5-diphenyltetrazolium bromide (MTT), dimethyl sulfoxide (DMSO), N-acetyl cysteine (NAC), and AKT inhibitor MK-2206 were purchased from Sigma (St. Louis, MO). Apoptosis Detection Kit Annexin V FITC and propidium iodide (PI) were purchased from BD Pharmingen. Antibodies, anti-MDM-2, anti-CDC2, anti-Cyclin B1, anti-p53, anti-Bcl-2, anti-Bax, anti-BAD, anti-caspase-3p30/17, anti-cleaved PARP, anti-PTEN, anti-p-PERK, anti-eIF2α, anti-ATF6, anti-XBP-1, anti-p-Akt, anti-p-mTOR, anti-GAPDH, goat anti-mouse IgG-HRP (horse-radish peroxidase), donkey anti-rabbit IgG-HRP and donkey anti-goat IgG-HRP were purchased from Santa Cruz Biotechnology (Santa Cruz, CA, USA). Anti-CHOP and anti-ATF4 antibodies were purchased from Cell Signaling Technology (Danvers, MA). Caspase-3 activity kit, ROS detection kit, JC-1 fluorescence probe and membrane-permeable calcium indicator fluo-3-acetoxymethyl (AM) ester were obtained from Beyotime Institute of Biotechnology (Shanghai, China).

2.2 WZ37 synthesis

The curcumin analog, WZ37, was synthesized by our laboratory and structurally identified by using mass spectrometry and ^{1}H nuclear magnetic resonance analysis (Wang et al., 2015). Briefly, the vanillin and 3,4-dihydro-2H-pyran are stirred in the dichloromethane, with PPTS as a catalyst, at room temperature for 5 h. This reaction mixture was purified by chromatography on silica gel to afford 3-methoxy-4-((tetrahydro-2H-pyran-2-yl)oxy)benzaldehyde. Aqueous NaOH solution (20% w/v, 5 ml) was added to a solution of 3-methoxy-4-((tetrahydro-2H-pyran-2-yl)oxy)benzaldehyde in acetone (20 ml). The reaction mixture was stirred at room temperature for 5-6 h to obtain the second intermediate, which

further reacted with 2,4,6-trimethyl-benzaldehyde in mixed suspension (10 ml) containing sodium hydroxide powder and dioxane. The reaction mixture was stirred at room temperature for 6 h, then purified by the chromatography on silica gel to afford (1E,4E)-1-(3-methoxy-4-((tetrahydro-2H-pyran-2-yl)oxy)phenyl)-5-(2',4',6'-trimethylphenyl) penta-1,4-dien-3-one. Finally, 5% HCl (1 ml) was added dropwise with stirring, and the end product, WZ37, was filtered and washed with water and dried in vacuum. Before using, compounds were recrystallized from $CHCl_3$/EtOH. HPLC evaluation determined the purity at >99%. The structure of WZ37 is shown in Figure 1A.

2.3 Cell lines and cell culture

The HNSCC cell lines, HEP-2 (Cat#: 3131C0001000700021), CNE-1 (Cat#: tw029125), CNE-2 (Cat#: 3142C0001000001303), CNE-2Z (Cat#: 3111C0001CCC000151) and 5-8F (Cat#: CM-H305), were purchased from Cell Bank of Shanghai Institutes [September, 2016; Biological Sciences, Chinese Academy of Sciences (Shanghai, China)]. The cells have been authenticated and tested for mycoplasma contamination by the Cell Bank of Shanghai Institutes using PCR assay. The cell lines were maintained in RPMI 1640 medium (Gibco, Eggenstein, Germany) supplemented with 10% heat-inactivated fetal bovine serum (FBS) (Hyclone, Logan, UT) and 0.2% of antibiotic solution (100 units/ml penicillin and 100 µg/ml streptomycin, Gibco, Invitrogen) at 37°C in a humidified atmosphere of 95% air and 5% CO_2 in an incubator (Thermo scientific).

2.4 Cell viability

Cell viability was assessed with the MTT assay. Briefly, the HEP-2, CNE-1, CNE-2, CNE-2Z and 5-8F cells were seeded at a density of 2500 cells per well in 96-well plates and allowed to attach overnight. On the following day, the cells were treated with increasing

concentrations of WZ37, curcumin, cisplatin (0.6, 1.25. 2.5, 5, 10, 20 and 40 μM) or with DMSO alone as solvent control for a period of 24 h. A 20 μl aliquot of MTT (5 mg/ml in PBS) was added to each well and incubated for 4 h. The medium was discarded, and 150 μl of DMSO was added to each well to dissolve the colored formazan crystals. After shaking for 10 min, the absorbance was measured at 495 nm in a microplate reader (Biotek Instruments, Inc., USA). Cell viability was expressed as a percentage of control groups and the IC_{50} was calculated as the concentration of drug required to obtain 50% maximal inhibition of cell viability.

2.5 Intracellular ROS measurement

The intracellular ROS content was determined using the dichlorofluorescein diacetate (DCFH-DA) reagent. In brief, HEP-2 (3×10^5 cells/well) were seeded in 6-well plates and allowed to attach overnight. After treatment with increasing concentrations of WZ37 (5, 15 and 25 μM) or DMSO alone as solvent control, cells were washed with serum-free RPMI 1640 and incubated with 1 μl (5 μM) of DCFH-DA at 37℃ for 30 min. In some experiments, HEP-2 cells were pre-treated with 5 mM NAC for 2 h prior to WZ37 exposure. The cells were harvested, washed with PBS, re-suspended in 1 ml PBS, and the fluorescent intensity was quantified by using FACS calibur flow cytometer (BD Biosciences, CA) analysed using FlowJo software (TreeStar, Ashland, OR, USA).

2.6 Determination of mitochondrial membrane potential (Δψm)

Mitochondrial transmembrane potential (Δψm) was detected using the JC-1 mitochondrial membrane potential assay kit. The HEP-2 cells were seeded at a density of 2×10^5 cells/dish in 30-mm culture dishes. After treatment with WZ37 (25 μM, 0-24 h), the cells were incubated with an equal volume of JC-1 staining solution (5 μg/ml) at 37°C for 20 min

and washed twice with JC-1 staining buffer. Fluorescence microscopy was used to monitor and record red emission of the fluorescent dye (indicating potential-dependent aggregation in mitochondria) and green fluorescence (indicating monomeric JC-1, appearing in the cytosol after mitochondrial membrane depolarization). Mitochondrial membrane potentials were determined by ratio of the green/red fluorescence intensity.

2.7 Measurement of free intracellular Ca^{2+} concentration

The free intracellular [Ca^{2+}] ([Ca^{2+}]$_i$) in HEP-2 cells was measured using a Ca^{2+}-sensitive fluorescence indicator, fluo-3-AM. Cells were treated with increasing concentrations of WZ37 (5, 15 and 25 μM) for 24 h or with WZ37 (25 μM) for different times (3, 9, or 24 h). Fluo-3 AM (5 μg/ml) was added to the cells and incubated for 30 min at 37°C. Then the cells were trypsinized, rinsed with PBS, re-suspended in 1 ml PBS, and the fluorescence intensity was quantified by using flow cytometry and analyzed using FlowJo software.

2.8 Cell cycle analysis

The cell-cycle distribution was determined by flow cytometric DNA analysis. HEP-2 cells were seeded at a density of 300,000 cells/well in 6-well plates and incubated overnight. On the following day, the cells were treated with increasing concentrations of WZ37 (5, 15 and 25 μM), curcumin (25 μM) or DMSO alone and incubated for 24 h. After treatment, the cells were harvested, washed twice with ice-cold PBS, fixed with 70% ethanol (2 h at −20°C). The cells were centrifuged to remove the ethanol, washed with cold PBS, suspended in 500 μl 1x PI staining solution and incubated at room temperature in the dark for 10 min. Flow cytometric analysis of cell cycle was conducted using FACS calibur flow cytometer and the data were analysed using FlowJo software.

2.9 Apoptosis determination

Apoptosis was determined using the Annexin V-FITC/PI apoptosis detection kit. The HEP-2 cells were plated as described for the cell cycle analysis. In some experiments, the cells were pre-treated with either 5 mM NAC for 2 h prior to WZ37 exposure, or with MK-2206 (10 μM) alone or in combination with WZ37 (25 μM) for 12 h. After treatment, cells were harvested and washed twice with ice-cold PBS, re-suspended in 500 μl binding buffer, stained with 3 μl FITC-conjugated anti-Annexin V for 10 min, and with 1 μl PI for 5 min. Apoptotic cells were measured using the FACS calibur flow cytometer and the data were analyzed using FlowJo software.

2.10 Caspase-3 activity assay

Caspase-3 activity was measured using Caspase-3 Activity Kit according to the manufacturer's instructions. Briefly, cells were treated using the same protocol as described for the cell cycle analysis. A cell lysis was made, which was centrifuged at 200,000×g for 15 min, and the protein concentration of the supernatant was determined by BCA protein assay. Ten μl of the supernatant was incubated with 10 μl Ac-DEVD-pNA (2 mM) for 2 h at 37°C in a 96-well microtitre plate. The release of p-nitroanilide (pNA) was quantified by determining the absorbance at 405 nm with the Multiskan Spectrum (Thermo) and the relative caspase-3 activity was calculated as a ratio of absorbance of treated cells to untreated cells.

2.11 Transmission electron microscopy (TEM)

The HEP-2 cells were seeded at a density of 6×10^5 cells/dish in 60-mm culture dishes and allowed to attach overnight. On the following day, the cells were treated with

WZ37 (25 μM), DMSO alone for 3 h or 24 h as solvent control. In some experiments, cells were pre-treated with 5 mM NAC for 2 h prior to WZ37 exposure. The cells were trypsinized, centrifuged and fixed in 2% glutaraldehyde in 0.1 M PBS (pH 7.4). Post-fixation was performed by incubating cells with 1% osmium tetroxide for 1 h at 4°C, followed by dehydration through a graded ethanol series, and embedded in epon. The embedded blocks were sectioned into semi-thin sections and stained with toluidine blue. Ultrathin sections were collected onto formvar-coated slot copper grids and counterstained with uranyl acetate and Reynolds lead citrate. Sections were observed by TEM (H-7500, Hitachi, Ibaraki, Japan).

2.12 Western blotting analysis

After indicated treatment protocol, the cells were washed with PBS, suspended in a protein lysis buffer under cold conditions, and cell debris was removed by centrifugation at 12,000 rpm for 10 min at 4 °C. Protein concentration of the samples was determined by the Bradford protein assay kit (Bio-Rad, Hercules, CA). The samples were separated on precast 8-15% SDS polyacrylamide gels and transferred to polyvinylidene difluoride (PVDF) membrane. The membranes were blocked with 5% non-fat dry milk in tris-buffered saline containing 0.1% Tween 20 (TBST) for 90 min at room temperature, and incubated with the specific primary antibody in TBST overnight at 4°C. The membranes were washed with TBST three times at 5 min intervals, incubated with HRP-conjugated secondary antibodies (1:4000) for 1 h at room temperature, and washed three times with TBST. Protein bands were detected using an enhanced chemiluminescence detection system (ECL, GE Healthcare), with detection of GAPDH as a loading control.

2.13 Statistical analysis

The experiments were made in triplicates (n=3), and the data are presented as means ± SEM. The statistical analyses were performed using GraphPad Pro. Prism 5.0 (GraphPad, San Diego, CA), with statistical differences between two groups assessed by Student's *t* test. A *P* value <0.05 was considered statistically significant.

3. Results

3.1 WZ37 inhibits cell viability of HNSCC

We have synthesized WZ37 with structural optimization for stability and improved anti-inflammatory potential (Materials and Methods). We first evaluated the effects of WZ37 on cell viability of panel of head and neck cancer cell lines (5-8F, CNE-1, CNE-2Z, CNE-2, HEP-2) using MTT assay. These cell lines are widely used for *in vitro* studies of HNSCC, including new drug discovery and identification of cellular mechanisms (Borges et al., 2017; Pozzi et al., 2015; Shen et al., 2011; Sun et al., 2015). We investigated the growth inhibitory potential of WZ37 by measuring its effects on viability of these HNSCC cell lines (Fig. 1B-1F). The parental compound, curcumin, and the clinical anti-cancer drug, cisplatin, were included for comparison with WZ37. As shown in Fig.1B-F, treatment with WZ37 for 24 h significantly inhibited viability of HNSCC in a dose-dependent manner. IC_{50} for WZ37 was consistently lower in all the HNSCC cell lines compared to those of curcumin and cisplatin. Interestingly, WZ37 inhibited viability most effectively in HEP-2 cells (IC_{50}=1.9±0.15 μM) among the cell lines studied, suggesting cell-selective sensitivity of WZ37 (Fig. 1F). Based on this greater sensitivity of HEP-2 cells to WZ37, the subsequent studies were made using HEP-2 cells.

3.2 WZ37 promotes cell cycle arrest and apoptosis

We investigated the effects of WZ37 on cell cycle arrest and apoptotic cascade as potential anti-cancer mechanisms in inhibiting HEP-2 cell growth. Analysis of the flow cytometric profile of Annexin V/PI staining indicated that WZ37 treatment for 24 h induced dose-dependent accumulation of apoptotic HEP-2 cells at early and late stages of apoptosis (Fig. 2A-B). WZ37 at 25 μM induced >40% of apoptotic cells, whereas curcumin at the same concentration, induced 20%, indicating the greater potency of WZ37. DMSO control cells showed low or negative staining with Annexin V FITC and PI, indicating viable cells (Fig. 2A-B). WZ37 treatment also increased the percentage of HEP-2 cells arrested at G2/M phase (Fig. 2C-D). Further, we determined the effects of WZ37 on apoptosis-related protein expressions by Western blotting. Results showed that WZ37 treatment for 24 h significantly increased expression of Bax, cleaved PARP and concomitantly decreased Bcl-2 and pro-caspase-3 (Fig. 2E), indicating pro-apoptotic changes. The pro-apoptotic profile of proteins was consistent with significant increase in caspase-3 activity in HEP-2 cells treated with WZ37 (Fig. 2F). Similarly, Western blot analysis of the effects of WZ37 on key proteins related to G2/M cell cycle arrest indicated decreased expression of MDM2, CDC2 and cyclin B1 (Fig. 2G). The effects of WZ37 (25 μM) on expression of apoptosis-related proteins and G2/M arrest were greater than that of curcumin at the same concentration (Fig. 2E and 2G), consistent with the observed greater potency of WZ37.

3.3 WZ37 induces ROS accumulation in HEP-2 cells

We next investigated whether the WZ37-inhibited cellular growth was attributed to intracellular ROS generation. ROS was measured by the common fluorescent probe DCFH-DA, which increases in fluorescence intensity in the presence of ROS. The treatment with WZ37 resulted in dose-dependent increases in the intracellular content of ROS in HEP-2 cells relative to DMSO control cells (Fig. 3A-B). Moreover, when cells were pre-treated with 5

mM NAC (ROS scavenger) for 2 h, the WZ37-induced intracellular accumulation of ROS was prevented (Figure 3C-D), confirming that WZ37 induced ROS production. More significantly, NAC pre-treatment abrogated the WZ37-induced apoptosis (Figure 3E-F) as well as the changes in expression of pro-apoptotic proteins (Figure 3G). The findings supported ROS as a mechanism by which WZ37 exerted its anti-cancer activity.

3.4 WZ37 induces endoplasmic reticulum (ER) stress in HEP-2 cells

Elevated intracellular levels of ROS are known stresses to the ER, which can lead to apoptosis. We investigated the involvement of potential ER stress in the WZ37-mediated anti-cancer activity. Cultured HEP-2 cells were treated with various time points (Fig. 4A) and doses (Fig. 4B), and expression of proteins associated with UPR was analysed by Western blotting analysis. Results indicated that WZ37 increased expression of UPR-associated proteins, i.e., p-PERK, p-EIF-2α, ATF-4, ATF6, XBp-1 and CHOP, with time- and dose-dependency (Fig. 4A-B), indicating activation of the UPR response by ER stress. WZ37 at 25 μM increased expression of the proteins to a greater extent than curcumin at the same concentration (Fig. 4B). We further evaluated the effects of WZ37 on the ultrastructure of ER. The results indicated that WZ37 induced enlargement and dilation of ER (Figure 4D), indicating ER injury and ER stress. Moreover, pre-treatment with NAC prevented the WZ37-induced increases in expression of UPR-associated proteins (Figure 4C) as well as the ER injury (Figure 4D). These results indicated that WZ37 induced ER stress as a consequence of ROS generation.

3.5 WZ37 increases $[Ca^{2+}]_i$, injures mitochondria, and impairs Akt /mTOR signaling

Early indices of cell stress, such as that in response to high levels of ROS, are mitochondrial injury and increased $[Ca^{2+}]_i$. We investigated the effects of WZ37 on $[Ca^{2+}]_i$ in

HEP-2 cells using the Fluo-Am fluorescent indicator. Results indicated that WZ37 (15 or 25 μM) treatment for 24 h significantly increased $[Ca^{2+}]_i$ (Figure 5A-B). Moreover, the WZ37 treatment induced mitochondrial membrane depolarization, which corresponded to the increased green fluorescence of the JC-1 probe (Figure 5C), indicating mitochondrial membrane depolarization and injury. In contrast, cells treated with WZ37 up to 12 h showed red fluorescent mitochondria, indicating intact mitochondrial membrane potential (Figure 5C). Ultrastructural examination of HEP-2 cells following 3 h of WZ37 treatment revealed mild ER swelling and normal mitochondria (Figure 5D). However, with 24 h of treatment, the extent of ER swelling increased which was accompanied by mitochondrial swelling with loss of crista (Figure 5D). Evidence indicates that the Akt/mTOR signalling cascade is important for normal mitochondrial homeostasis, as well as regulation of cell survival and apoptosis by targeting Bcl-2 family of proteins and PTEN, a negative regulator of Akt. We investigated whether Akt/mTOR was a target of regulation by WZ37 in HEP cells. Western blotting analysis indicated that WZ37 (25 μM) treatment for 24 h increased expression of BAD, a regulator of mitochondria-dependent apoptosis, as well as PTEN, and significant reduction of phosphorylation of Akt and mTOR (Figure 5E). The findings indicated that although WZ37 activated the Akt/mTOR pathway at early time points (3 h), the activation decayed by 24 h, indicating inhibition of the pathway. This latter effect of WZ37 corresponded with the peak expression of PTEN/BAD. The findings suggest that the later decreased Akt/mTOR activity likely contributed to the promotion of apoptosis.

3.6 Inhibition of oxidant-sensitive Akt/mTOR promotes apoptosis

We investigated the role of Akt/mTOR pathway in regulation of WZ37-induced apoptosis. Since our data indicated that WZ37 can induce production of ROS, we first determined whether ROS activated Akt/mTOR. Results indicated that pre-treatment of HEP-

2 cells with NAC for 2 h prevented the WZ37-induced increases of p-Akt and p-mTOR (Figure 6C). As expected, pre-treatment with MK-2206, an allosteric Akt inhibitor with broad preclinical antitumor activity, also inhibited the WZ37-induced increases of p-Akt and p-mTOR (Figure 6C), suggesting loss of important signals for regulating normal mitochondrial homeostasis and cell survival. Therefore, we hypothesized that the reduced Akt/mTOR signalling, such as that in response to MK-2206, would synergized with WZ37, leading to heightened apoptotic activity. The results showed that a combined treatment of WZ37 with MK-2206 caused 2-fold greater increase in apoptosis relative to either treatment alone (Figure 6A-B). These results support the notion that the oxidant-sensitive Akt/mTOR plays a significant pro-survival role in cancer cells.

4. Discussion

HNSCC contributes globally to a great number of deaths and morbidity. Despite continuous improvements in cancer detection techniques and management, HNSCC patients are still predominantly incurable due to the metastatic potential and drug resistance (Dunn et al., 2018). Therefore, there is much interest in developing targeted therapeutic agents for treatment of HNSCC. Curcumin is a multifunctional bioactive natural product with relatively safe and well-tolerated properties. In this study, we found that WZ37, a novel curcumin analog, effectively suppressed proliferation of several HNSCC cells lines. Our laboratory originally designed and discovered WZ37 as an anti-inflammatory compound based on structural modification of curcumin (Wang et al., 2015). Since curcumin has been shown to exhibit excellent anti-cancer effects *in vivo* and *in vitro*, we also tested WZ37 for its anti-cancer effects. Interestingly, the WZ37 IC_{50} values were lower than that of either the parental compound curcumin or cisplatin in almost all examined cell lines, indicating the greater potency of WZ37 in cancer treatment. These were new findings pointing to WZ37 as a

potential highly effective anti-cancer agent for treatment of HNSCC, therefore, we investigated the cellular and molecular mechanisms by which WZ37 inhibited cancer cell growth.

There is a great need of new drugs that are therapeutically effective to HNSCC. Curcumin, which is the principal active ingredient of the traditional Chinese herb *Curcuma Longa*, has inhibitory effects on proliferation and survival of HNSCC. Curcumin induces cytotoxicity, apoptosis, and cell cycle arrest in G_2/M phase in HSNCC cell lines. Recently, Hu et al. (Hu et al., 2017) found that curcumin induces G2/M cell cycle arrest and apoptosis of HNSCC *in vitro* and *in vivo* through ATM/Chk2/p53-dependent pathway. This group also showed that anticancer activity of curcumin was associated with SIRT1 activation in HNSCC cell lines (Hu et al., 2015). While our study did not test the reported signalling pathway by which curcumin exerted anti-HNSCC activity, we observed that WZ37 had lower IC_{50} values compared to curcumin, as evaluated by the MTT assay (Figure 1), indicating higher anti-cancer ability of WZ37 than that of curcumin. Thus, we further investigated the anti-cancer mechanism of WZ37 in HNSCC cells.

Several cellular stresses are known to activate the ER stress response, UPR, that could lead to apoptosis (Song et al., 2017). We found that WZ37 induced a rapid production of ROS in HEP2 cells, in which an elevated and persistent intracellular ROS content was maintained for up to 24 h. This was accompanied by increased expression of PERK, ATF6 and XBP-1 (downstream of IRE), indicating activation of UPR. Studies have reported that the PERK/eIF2α/ATF4 axis is likely a predominant participant of ER stress-induced apoptosis via up-regulating the pro-apoptotic transcription factor, CHOP (Nabavi et al., 2018). Our data indicated that WZ37 treatment was associated with increased CHOP expression, implicating that elevated ROS induced cell death through a mechanism of ER stress.

Mitochondria are dynamic organelles whose proper function is fundamentally important for the viability of cells. Mitochondrial dysfunction can also lead to mitochondrial-dependent apoptosis initiated by interactions of CHOP with pro-apoptotic proteins in the BCL-2 family, such as BAD and BAX. The result of this complex interaction impairs the integrity of the mitochondrial outer membrane, leading to increased mitochondrial membrane permeability, release of free Ca^{2+}, activation of aspartate-specific proteases and the caspases, and ultimately apoptosis (Deegan et al., 2015; Shen et al., 2017; Vavilis et al., 2016). We observed that WZ37 treatment in HEP-2 cells increased the cytosolic [Ca^{2+}] by 24 h, which was associated with mitochondrial membrane depolarization, an indication of mitochondrial injury. Subsequent TEM results demonstrated that cells treated with WZ37 developed mitochondrial swelling, corroborating the loss of membrane potential. These data provide evidence that ROS-induced mitochondrial dysfunction contributed to apoptosis in response to WZ37 treatment.

The Akt/mTOR pathway is an important cellular communication cascade that cross-talks with a variety of other signalling pathways to regulate cell survival (Wani et al., 2016; Xu et al., 2017). Studies indicated that the Akt/mTOR pathway is highly activated and over-expressed in most cancers (Huang et al., 2017). Evidence indicates that AKT/mTOR decreases expression of pro-apoptotic BAD, thereby together with the anti-apoptotic members of the BCL-2 family, promotes a protective effect on mitochondrial membrane for cell survival (Zhang et al., 2017). Our data indicated that the WZ37-induced apoptosis of HEP2 cells was through decreased activity of AKT/mTOR at 24 h, which was accompanied by elevated expression of BAD. The results suggested that decreased AKT/mTOR signalling contributed to the regulation of apoptosis in response to WZ37. This possibility was further supported by the finding that when WZ37 treatment was combined with MK-2206, the Akt inhibitor, apoptosis of HEP2 cells was significantly enhanced compared to WZ37 alone.

Moreover, NAC pre-treatment prevented the WZ-37-induced activation of Akt/mTOR, indicating oxidant-sensitivity. The findings support an oxidant-dependent mechanism of apoptosis regulated by ER stress signals, mitochondrial dysfunction, and loss of Akt/mTOR survival signalling. Thus, WZ37 in combination with Akt/mTOR-selective inhibitors could provide a promising new therapeutic regimen for cancers such as HNSCC.

5. Conclusions

In summary, results from our study indicated that the curcumin analog, WZ37, was highly effective in inducing apoptosis of several HNSCC cell lines. Moreover, the apoptosis was oxidant-dependent and regulated by ER stress signals, mitochondrial dysfunction, and loss of Akt/mTOR survival signalling. Since this work was focused only on the cellular mechanism of WZ37, further studies are necessary to validate this concept at the animal level and to evaluate the preclinical pharmacodynamics and safety of WZ37 as an anti-cancer candidate. These mechanistic insights of WZ37, along with improved stability and enhanced anti-cancer potency over the parental compound, curcumin, provide strong support for the novel WZ37 as a potential candidate for treatment of HNSCC.

Supplementary file

Supplemental information includes 2 figures and can be found with this article online.

Acknowledgements

We kindly thank Professor Hazel Lum (Rush University, Chicago, IL) for language editing of the manuscript.

This study was supported by Science Foundation of Zhejiang Province (LR18H160003 to Y.Wang; LQ18H280007 to F. Lin), and National Natural Science Foundation of China (81803781 to F. Lin; 81672627 to X. Zhang; 21572167 to C. Li; 81603153 to Y. Xia).

Conflict of interest

The authors declare that they have no competing interests.

Authors' contributions

All authors have read and approved the submission of this manuscript; Z.Z., R.L., Y.X., L.Z., F.L., and X.Z. performed the research; G.L. and B.H. designed the research study; Y.Z., C.L., and L.W. contributed essential reagents or tools; L.W., B.H., and L.Z. analyzed the data; G.L. and B.H. wrote the paper.

References

Borges, G.A., Rego, D.F., Assad, D.X., Coletta, R.D., De Luca Canto, G., Guerra, E.N., 2017. In vivo and in vitro effects of curcumin on head and neck carcinoma: a systematic review. J Oral Pathol Med 46, 3-20.

Capodanno, Y., Buishand, F.O., Pang, L.Y., Kirpensteijn, J., Mol, J.A., Argyle, D.J., 2018. Notch pathway inhibition targets chemoresistant insulinoma cancer stem cells. Endocr Relat Cancer 25:131-144.

Deegan, S., Koryga, I., Glynn, S.A., Gupta, S., Gorman, A.M., Samali, A., 2015. A close connection between the PERK and IRE arms of the UPR and the transcriptional regulation of autophagy. Biochem Biophys Res Commun 456, 305-311.

Dunn, L.A., Fury, M.G., Xiao, H., Baxi, S.S., Sherman, E.J., Korte, J., Pfister, C., Haque, S., Katabi, N., Ho, A.L., Pfister, D.G., 2018. A phase II study of temsirolimus added to low-dose weekly carboplatin and paclitaxel for patients with recurrent and/or metastatic (R/M) head and neck squamous cell carcinoma (HNSCC). Ann Oncol 29: 1606.

Ho, A.S., Kim, S., Tighiouart, M., Gudino, C., Mita, A., Scher, K.S., Laury, A., Prasad, R., Shiao, S.L., Ali, N., Patio, C., Mallen-St Clair, J., Van Eyk, J.E., Zumsteg, Z.S., 2017. Association of Quantitative Metastatic Lymph Node Burden With Survival in Hypopharyngeal and Laryngeal Cancer. JAMA Oncol 4:985-989.

Hou, L., Wei, L., Zhu, S., Wang, J., Quan, R., Li, Z., Liu, J., 2017. Avian metapneumovirus subgroup C induces autophagy through the ATF6-UPR pathway. Autophagy 13, 1709-1721.

Hu, A., Huang, J.J., Li, R.L., Lu, Z.Y., Duan, J.L., Xu, W.H., Chen, X.P., Fan, J.P., 2015. Curcumin as therapeutics for the treatment of head and neck squamous cell carcinoma by activating SIRT1. Sci Rep 5, 13429.

Hu, A., Huang, J.J., Zhang, J.F., Dai, W.J., Li, R.L., Lu, Z.Y., Duan, J.L., Li, J.P., Chen, X.P., Fan, J.P., Xu, W.H., Zheng, H.L., 2017. Curcumin induces G2/M cell cycle arrest and apoptosis of head and neck squamous cell carcinoma in vitro and in vivo through ATM/Chk2/p53-dependent pathway. Oncotarget 8, 50747-50760.

Huang, J., Liu, Z., Xu, P., Zhang, Z., Yin, D., Liu, J., He, H., He, M., 2017. Capsaicin prevents mitochondrial damage, protects cardiomyocytes subjected to anoxia/reoxygenation injury mediated by 14-3-3eta/Bcl-2. Eur J Pharmacol 819, 43-50.

Kupsco, A., Schlenk, D., 2015. Oxidative stress, unfolded protein response, and apoptosis in developmental toxicity. Int Rev Cell Mol Biol 317, 1-66.

Leone, C.A., Capasso, P., Topazio, D., Russo, G., 2016. Supracricoid laryngectomy for recurrent laryngeal cancer after chemoradiotherapy: a systematic review and meta-analysis. Acta Otorhinolaryngol Ital 36, 439-449.

Nabavi, S.M., Russo, G.L., Tedesco, I., Daglia, M., Orhan, I.E., Nabavi, S.F., Bishayee, A., Nagulapalli Venkata, K.C., Abdollahi, M., Hajheydari, Z., 2018. Curcumin and Melanoma: From Chemistry to Medicine. Nutr Cancer, 1-12.

Nicco, C., Batteux, F., 2017. ROS Modulator Molecules with Therapeutic Potential in Cancers Treatments. Molecules 23 :pii:E84.

Poorghorban, M., Das, U., Alaidi, O., Chitanda, J.M., Michel, D., Dimmock, J., Verrall, R., Grochulski, P., Badea, I., 2015. Characterization of the host-guest complex of a curcumin analog with beta-cyclodextrin and beta-cyclodextrin-gemini surfactant and evaluation of its anticancer activity. Int J Nanomedicine 10, 503-515.

Pozzi, V., Sartini, D., Rocchetti, R., Santarelli, A., Rubini, C., Morganti, S., Giuliante, R., Calabrese, S., Di Ruscio, G., Orlando, F., Provinciali, M., Saccucci, F., Lo Muzio, L., Emanuelli, M., 2015. Identification and characterization of cancer stem cells from head and neck squamous cell carcinoma cell lines. Cell Physiol Biochem 36, 784-798.

Rayess, H.M., Xi, Y., Garshott, D.M., Brownell, A.L., Yoo, G.H., Callaghan, M.U., Fribley, A.M., 2018. Benzethonium chloride activates ER stress and reduces proliferation in HNSCC. Oral Oncol 76, 27-33.

Senft, D., Ronai, Z.A., 2015. UPR, autophagy, and mitochondria crosstalk underlies the ER stress response. Trends Biochem Sci 40, 141-148.

Shen, B., Dong, P., Li, D., Gao, S., 2011. Expression and function of ABCG2 in head and neck squamous cell carcinoma and cell lines. Exp Ther Med 2, 1151-1157.

Shen, Y.Q., Guerra-Librero, A., Fernandez-Gil, B.I., Florido, J., Garcia-Lopez, S., Martinez-Ruiz, L., Mendivil-Perez, M., Soto-Mercado, V., Acuna-Castroviejo, D., Ortega-Arellano, H., Carriel, V., Diaz-Casado, M.E., Reiter, R.J., Rusanova, I., Nieto, A., Lopez, L.C., Escames, G., 2018. Combination of melatonin and rapamycin for head and neck cancer therapy: Suppression of AKT/mTOR pathway activation, and activation of mitophagy and apoptosis via mitochondrial function regulation. J Pineal Res. 64(3).

Shpilka, T., Haynes, C.M., 2018. The mitochondrial UPR: mechanisms, physiological functions and implications in ageing. Nat Rev Mol Cell Biol. 19:109-120.

Song, S., Tan, J., Miao, Y., Zhang, Q., 2018. Crosstalk of ER stress-mediated autophagy and ER-phagy: Involvement of UPR and the core autophagy machinery. J Cell Physiol 233: 3867-3874.

Sun, S.S., Zhou, X., Huang, Y.Y., Kong, L.P., Mei, M., Guo, W.Y., Zhao, M.H., Ren, Y., Shen, Q., Zhang, L., 2015. Targeting STAT3/miR-21 axis inhibits epithelial-mesenchymal transition via regulating CDK5 in head and neck squamous cell carcinoma. Mol Cancer 14, 213.

Vavilis, T., Delivanoglou, N., Aggelidou, E., Stamoula, E., Mellidis, K., Kaidoglou, A., Cheva, A., Pourzitaki, C., Chatzimeletiou, K., Lazou, A., Albani, M., Kritis, A., 2016. Oxygen-Glucose Deprivation (OGD) Modulates the Unfolded Protein Response (UPR) and Inflicts Autophagy in a PC12 Hypoxia Cell Line Model. Cell Mol Neurobiol 36, 701-712.

Wang, Z., Zou, P., Li, C., He, W., Xiao, B., Fang, Q., Chen, W., Zheng, S., Zhao, Y., Cai, Y., Liang, G., 2015. Synthesis and biological evaluation of novel semi-conservative mono-carbonyl analogs of curcumin as anti-inflammatory agents. MedChemComm 6, 1328-1339.

Wani, Z.A., Guru, S.K., Rao, A.V., Sharma, S., Mahajan, G., Behl, A., Kumar, A., Sharma, P.R., Kamal, A., Bhushan, S., Mondhe, D.M., 2016. A novel quinazolinone chalcone derivative induces mitochondrial dependent apoptosis and inhibits PI3K/Akt/mTOR signaling pathway in human colon cancer HCT-116 cells. Food Chem Toxicol 87, 1-11.

Xu, L., Xie, Q., Qi, L., Wang, C., Xu, N., Liu, W., Yu, Y., Li, S., Xu, Y., 2018. Bcl-2 overexpression reduces cisplatin cytotoxicity by decreasing ER-mitochondrial Ca2+ signaling in SKOV3 cells. Oncol Rep 39: 985-992.

Yamazaki, H., Suzuki, G., Nakamura, S., Hirano, S., Yoshida, K., Konishi, K., Teshima, T., Ogawa, K., 2017. Radiotherapy for locally advanced resectable T3-T4 laryngeal cancer-does laryngeal preservation strategy compromise survival? J Radiat Res, 1-14.

Zhang, W., Xue, X., Fu, T., 2017. Construction of a Bcl-2-shRNA expression vector and its effect on the mitochondrial apoptosis pathway in SW982 cells. Int J Mol Med 40, 1914-1920.

Zou, P., Zhang, J., Xia, Y., Kanchana, K., Guo, G., Chen, W., Huang, Y., Wang, Z., Yang, S., Liang, G., 2015. ROS generation mediates the anti-cancer effects of WZ35 via activating JNK and ER stress apoptotic pathways in gastric cancer. Oncotarget 6, 5860-5876.

Figure Legends

Figure 1. WZ37 inhibits cell viability of HNSCC in a dose-dependent manner

(A) The structure of WZ37 and curcumin (CUR). Cell viability was assayed using the MTT reagent (Methods) on several HNSCC cell lines: **(B)** 5-8F, **(C)** CNE-1, **(D)** CNE-2Z, **(E)** CNE-2 and **(F)** HEP-2. The cells were treated with a range of concentrations (0.625, 1.25, 2.5, 5, 10, 20, 40 μM) of WZ37, curcumin or cisplatin for 72 h, and viability reported as % cell survival and IC_{50}. Values were presented as means ± SEM from three individual experiments.

Figure 2. WZ37 promotes apoptosis and cell cycle arrest in HEP-2 cells

HEP-2 cells were treated with WZ37 (5, 15, or 25 μM) or curcumin (CUR; 25 μM) for 24 h, and analyzed as described below. **(A)** The treated cells were stained with Annexin V-FITC/propidium iodide (Methods); shown are representative cytometric graphs of apoptotic cells. **(B)** Quantification of the number of dead cells obtained in (A). **(C)** For cell cycle arrest analysis, treated cells were stained with propidium iodide; shown are representative graphs of number of HEP-2 cells arrested at G2/M as analyzed by flow cytometry. **(D)** Quantification of arrested cells obtained in (C). **(E)** Treated HEP-2 cells were prepared for Western blot analysis for detection of apoptosis-related proteins. Shown are representative blots from 3 separate determinations; GAPDH was used as internal control. **(F)** The treated HEP2 cells were measured for caspase-3 activity using the substrate Ac-LEVD-pNA (Methods): the relative caspase-3 activity was calculated as a ratio of treated cells to untreated cells. **(G)** Shown is a representative Western blot analysis for detection of proteins related with G2/M cell cycle regulation; 3 separate determinations; GAPDH was used as internal control. B, D, and F: values reported as mean ± SEM; n = 3; *$P < 0.05$, ** $P < 0.01$, and ***$P < 0.001$.

Figure 3. WZ37 induces ROS accumulation in HEP-2 cells

(A) The effects of WZ37 on ROS production in HEP-2 cells were determined using the DCFH-DA fluorescent probe and detection by flow cytometry analysis (Methods); shown is a representative cytometric graph of DCFH fluorescence (indicator of ROS content) in HEP2 cells treated with WZ37 at the indicated concentrations. **(B)** Quantification of the DCFH fluorescence obtained from (A); values represented as the medium of relative fluorescence intensity. **(C)** The effects of pre-treatment with NAC (5 mM for 2 h), an anti-oxidant, on WZ37-induced ROS production were determined; shown is representative cytometric graph of DCFH fluorescence in HEP-2 cells. **(D)** Quantification of the flow cytometric analysis obtained in (C); values were calculated and represented as the medium of relative fluorescence intensity. **(E)** The effects of NAC pre-treatment (5 mM for 2 h) on WZ37-induced apoptosis were determined with Annexin V-FITC/propidium iodide stain and the rates of apoptotic cells were detected by flow cytometry; shown are representative graphs of apoptotic cells from treatment groups. **(F)** Quantification of the number of dead cells from analysis in (E); values represented as % apoptotic cells. **(G)** Representative Western blot analysis of the effects of NAC pre-treatment (5 mM for 2 h) of HEP-2 cells on expression of apoptosis-related proteins; 3 separate determinations. B, D, and F: values reported as mean $\pm$ SEM; n = 3; $^{*}P < 0.05$, $^{**}P < 0.01$ vs DMSO group; $^{\#\#}P < 0.01$ vs WZ37 group.

Figure 4. WZ37 induces endoplasmic reticulum (ER) stress in HEP-2 cells

Effects of WZ37 on ER stress response was determined in HEP-2 cells. Cells were treated with WZ37 or curcumin (Cur) at the indicated time **(A)** and doses **(B)**, or HEP-2 cells were pre-treated with NAC (5 mM for 2 h) before exposure to WZ37 (25 μM) for 6 h **(C)**, and ER stress-related proteins were detected by Western blot analysis; shown is representative blot

from 3 separate determinations; GAPDH was loading control. **(D)** The treated HEP-2 cells were also evaluated for effects of WZ37 on ultrastructural changes of ER and mitochondria. Black arrowheads indicate mitochondria and red arrowheads the ER; magnification × 20,000; 3 separate determinations.

Figure 5. WZ37 impairs Ca^{2+} homeostasis, mitochondrial function, and the Akt /mTOR survival cascade

The effects of WZ37 on Ca^{2+} homeostasis and mitochondrial function were determined in HEP2 cells treated with WZ37 at the indicated concentrations and times. **(A)** Intracellular Ca^{2+} concentration ($[Ca^{2+}]_i$) was measured using the Ca^{2+} indicator fluorescent dye, Fluo 3/AM (5 μg/ml) (Methods) and analyzed by flow cytometry; shown are representative graphs of Fluo fluorescence, indicating changes of $[Ca^{2+}]_i$. **(B)** Quantification of the $[Ca^{2+}]_i$ in HEP-2 cells; values represent as the medium of relative fluorescence intensity; n = 3; values reported as mean ± SEM; $^{**}P < 0.01$ compared to DMSO control. **(C)** Mitochondrial membrane potential was determined to evaluate the effects of WZ37 on mitochondrial function. The treated cells were stained with the fluorescent JC-1 membrane potential probe, and evaluated by fluorescent microscopy. Red fluorescence represents a potential-dependent mitochondrial aggregation, indicating intact mitochondrial membrane. Green fluorescence indicates monomeric form of JC-1, indicating mitochondrial membrane depolarization; shown is representative images from 3 separate determinations. **(D)** Mitochondrial ultrastructural changes were evaluated from HEP-2 cells treated with WZ37 (25 μM) for 3 h or 24 h; black arrowheads indicate mitochondria, and red arrowheads indicate ER; TEMs are representative of 3 separate determinations; magnification ×20,000. **(E)** Effects of WZ37 or curcumin (Cur) on expression of proteins of the AKT/mTOR and pro-apoptotic UPR pathways were determined by Western blot analysis of HEP-2 cells treated with WZ37 (25 μM) at the

indicated times or indicated doses for 24 h; shown is representative blot from 3 separate determinations; GAPDH was used as loading control.

Figure 6. Inhibition of oxidant-sensitive Akt/mTOR promotes apoptosis

The role of AKT/mTOR signaling in regulation of the WZ37-induced apoptosis was investigated with the Akt inhibitor, MK-2206, in HEP2 cells. Cells were treated with a combination of WZ37 (25 μM) and MK-2206 (10 μM), or either reagents alone for 24 h. **(A)** Shown is representative cytometric analysis of apoptotic cells from each treatment group. **(B)** Quantification of apoptotic cells determined from (A); values reported as % apoptotic cells as mean ± SEM; n = 3; * $P<0.05$, ** $P<0.01$, compared to DMSO control. **(C)** The treated HEP-2 cells were analysed for expression of proteins of the AKT/mTOR pathway; shown is representative Western blot analysis from 3 separate determinations; GAPDH was used as loading control.

Curcumin analog, WZ37, promotes G2/M arrest and apoptosis of HNSCC cells through Akt/mTOR inhibition

Ziheng Zhang[1,2,3,#], Renyu Lin,[1,2,#], Zhoudi Liu[1], Tao Yan[1], Yiqun Xia[2], Leping Zhao[3], Feng Lin[2], Xi Zhang[3], Chenglong Li[1], Yi Wang[1,*]

[1] Chemical Biology Research Center, School of Pharmaceutical Sciences, Wenzhou Medical University, Wenzhou, Zhejiang 325035, China

[2] The First Affiliated Hospital of Wenzhou Medical University, Wenzhou, Zhejiang 325035, China

[3] Department of Pharmacy, the Affiliated Yueqing Hospital of Wenzhou Medical University, Wenzhou, Zhejiang 325000, China

Highlights:

1. New targeted therapies are in urgent needed for NHSCC treatment.
2. WZ37 inhibited proliferation of several HNSCC cell types by G2/M cycle arrest.
3. WZ37 induced ROS dependent mitochondrial injury and ER stress.
4. The anti-cancer effect of WZ37 was due to inhibition of the Akt/mTOR pathway.
5. WZ37 can be a promising anti-cancer agent for the treatment of HNSCC.

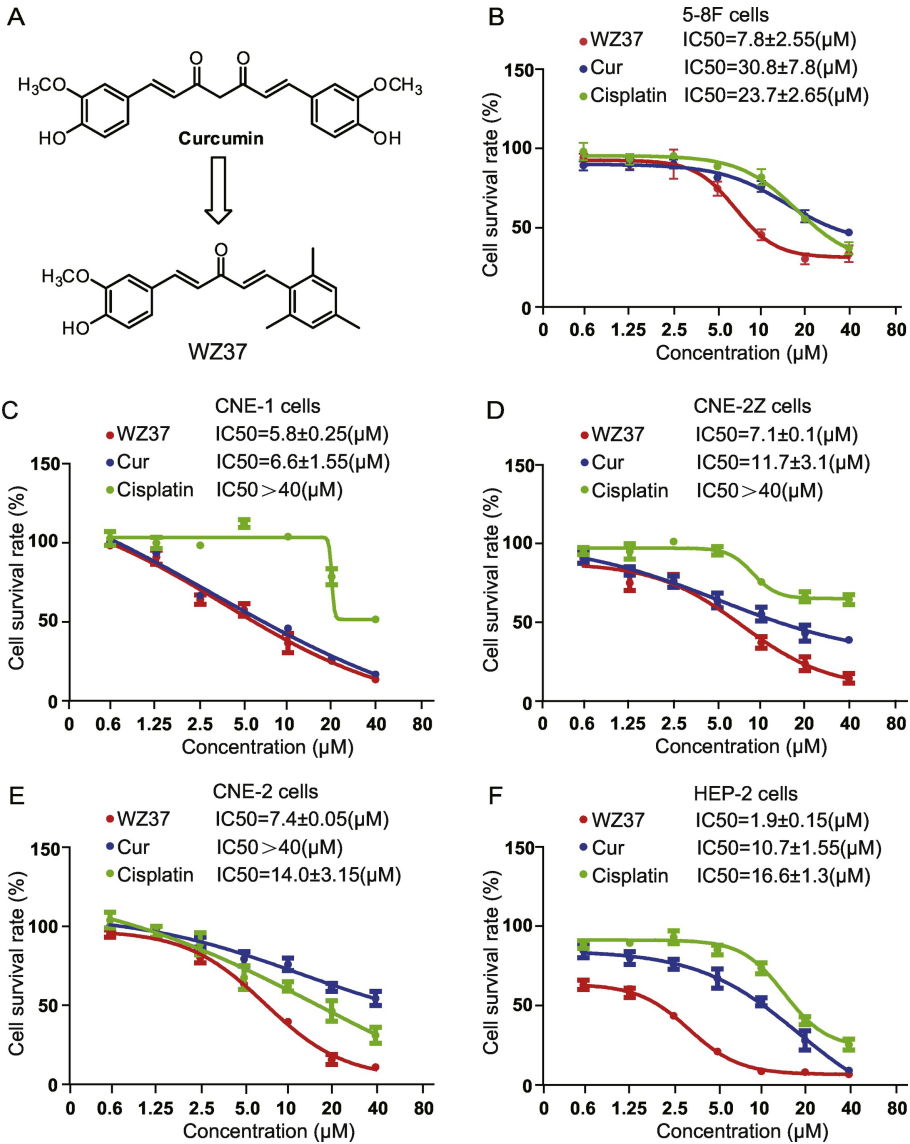
A
Curcumin
WZ37
B
5-8F cells
WZ37 IC50=7.8±2.55(μM)
Cur IC50=30.8±7.8(μM)
Cisplatin IC50=23.7±2.65(μM)
C
CNE-1 cells
WZ37 IC50=5.8±0.25(μM)
Cur IC50=6.6±1.55(μM)
Cisplatin IC50＞40(μM)
D
CNE-2Z cells
WZ37 IC50=7.1±0.1(μM)
Cur IC50=11.7±3.1(μM)
Cisplatin IC50＞40(μM)
E
CNE-2 cells
WZ37 IC50=7.4±0.05(μM)
Cur IC50＞40(μM)
Cisplatin IC50=14.0±3.15(μM)
F
HEP-2 cells
WZ37 IC50=1.9±0.15(μM)
Cur IC50=10.7±1.55(μM)
Cisplatin IC50=16.6±1.3(μM)
Cell survival rate (%)
Concentration (μM)

Figure 1

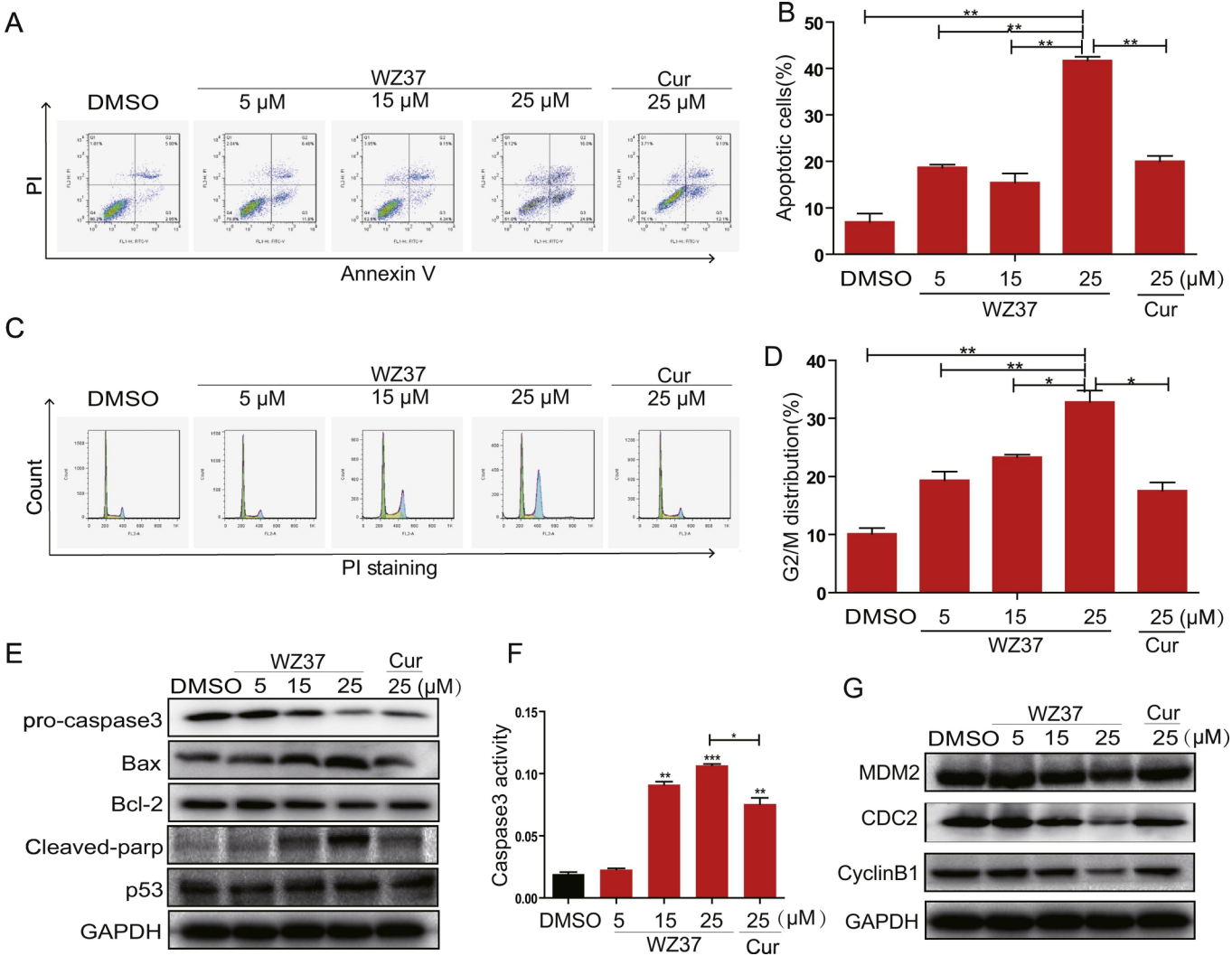
A
DMSO
WZ37
5 μM
15 μM
25 μM
Cur
25 μM
PI
Annexin V
B
Apoptotic cells(%)
DMSO
5
15
25
25 (μM)
WZ37
Cur
C
Count
PI staining
D
G2/M distribution(%)
E
pro-caspase3
Bax
Bcl-2
Cleaved-parp
p53
GAPDH
F
Caspase3 activity
G
MDM2
CDC2
CyclinB1
GAPDH

Figure 2

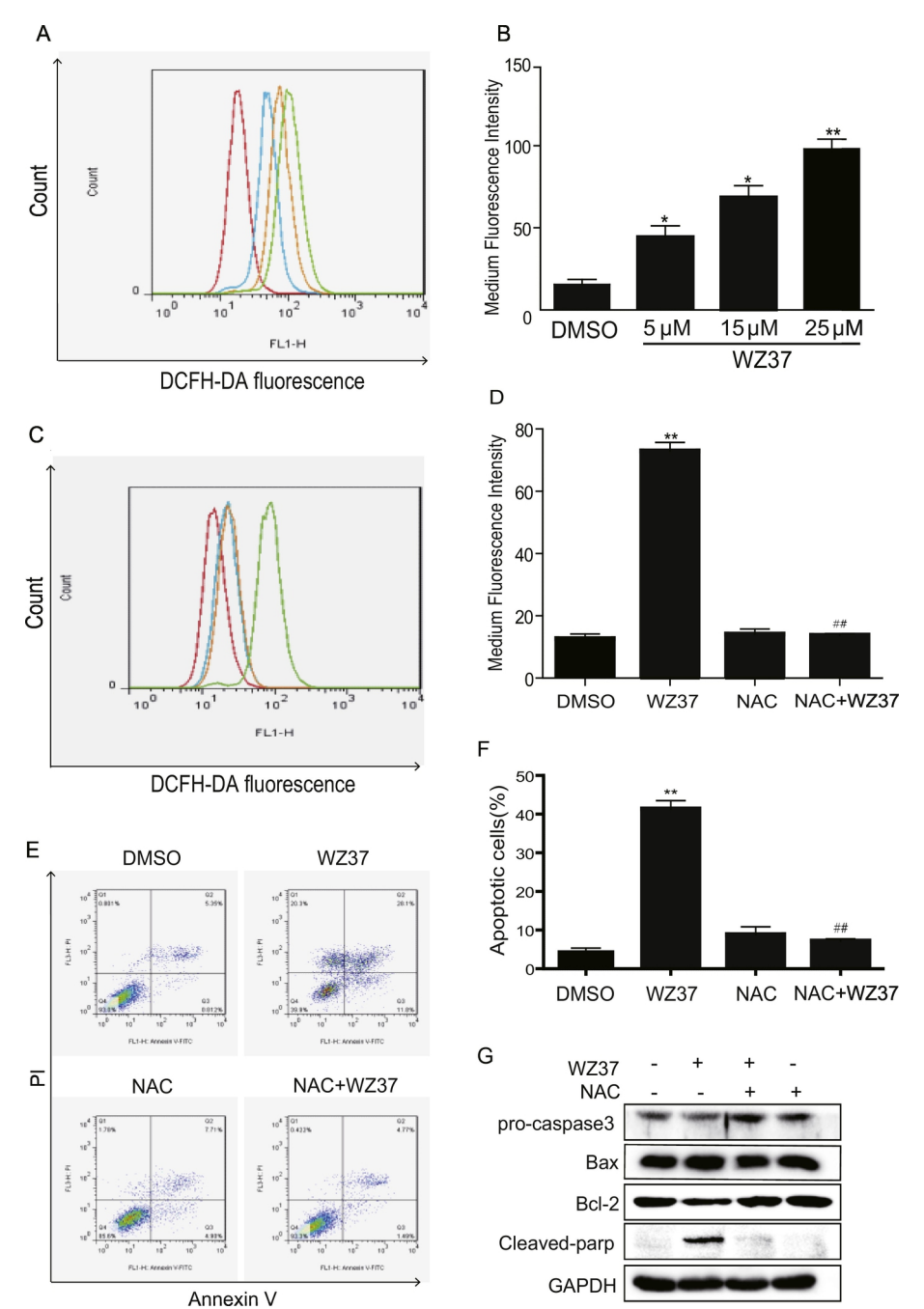
A
Count
Count
FL1-H
DCFH-DA fluorescence
B
Medium Fluorescence Intensity
150
100
50
0
*
*
**
DMSO
5 μM
15 μM
25 μM
WZ37
C
Count
Count
FL1-H
DCFH-DA fluorescence
D
Medium Fluorescence Intensity
80
60
40
20
0
**
##
DMSO
WZ37
NAC
NAC+WZ37
E
DMSO
WZ37
NAC
NAC+WZ37
PI
Annexin V
F
Apoptotic cells(%)
50
40
30
20
10
0
**
##
DMSO
WZ37
NAC
NAC+WZ37
G
WZ37 - + + -
NAC - - + +
pro-caspase3
Bax
Bcl-2
Cleaved-parp
GAPDH

Figure 3

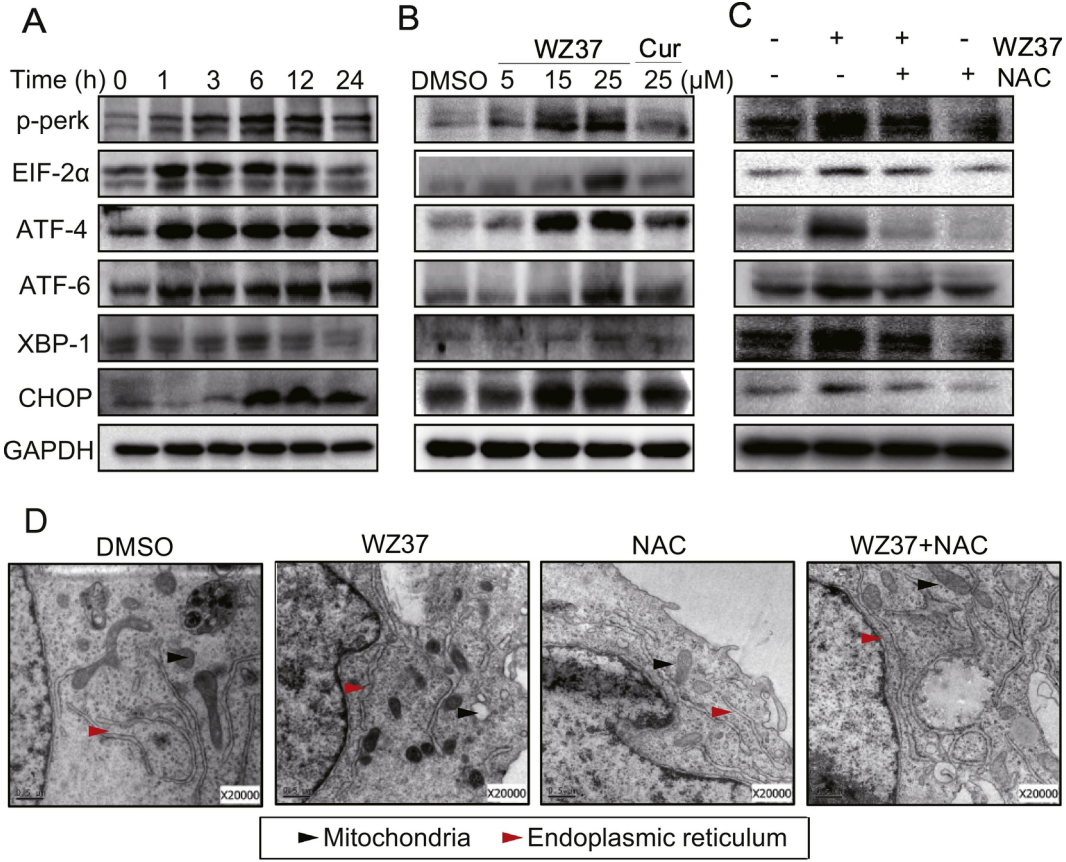
A
Time (h) 0 1 3 6 12 24
p-perk
EIF-2α
ATF-4
ATF-6
XBP-1
CHOP
GAPDH
B
WZ37
Cur
DMSO 5 15 25 25 (μM)
C
- + + - WZ37
- - + + NAC
D
DMSO
WZ37
NAC
WZ37+NAC
x20000
Mitochondria
Endoplasmic reticulum

Figure 4

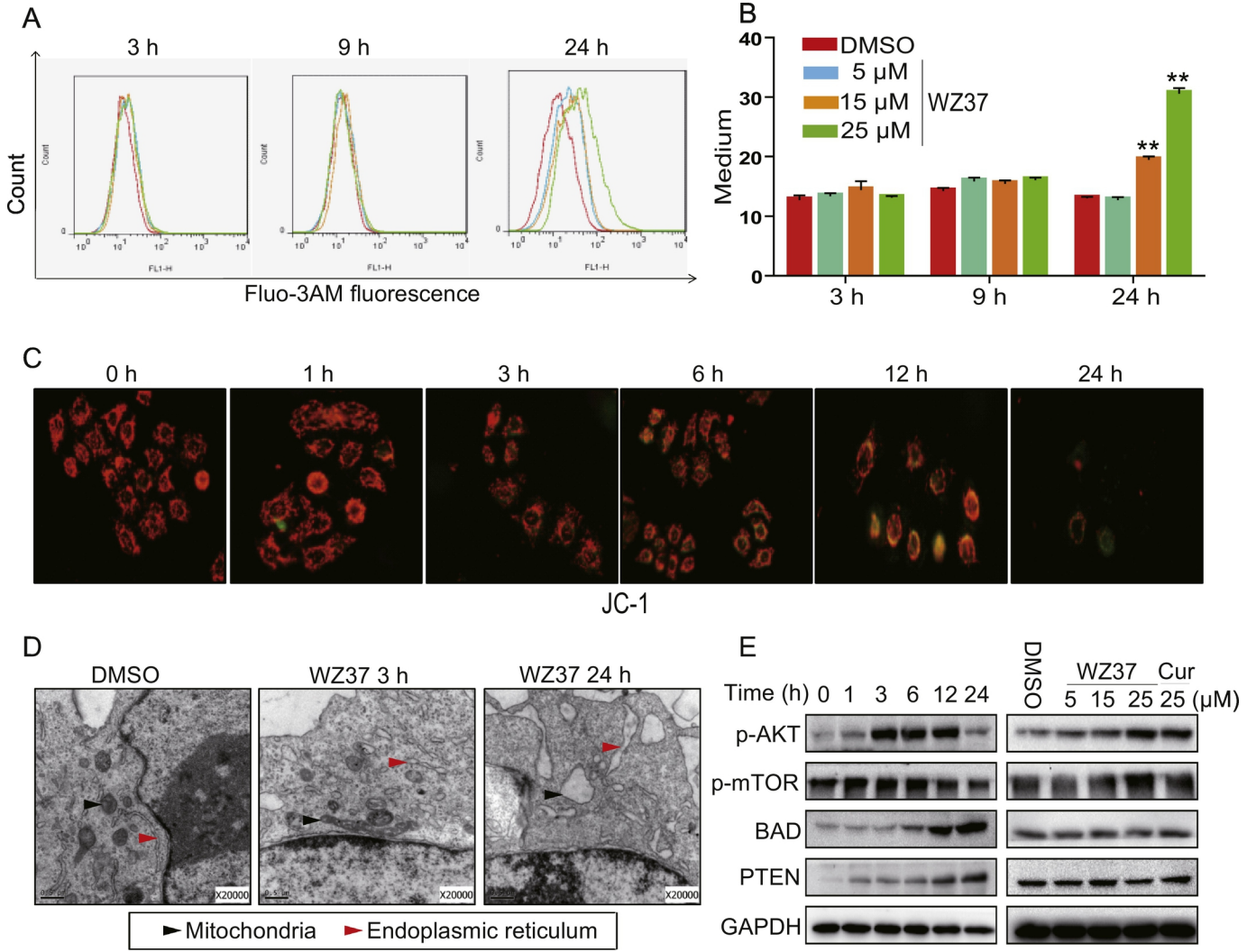
A
3 h
9 h
24 h
Count
FL1-H
Fluo-3AM fluorescence
B
DMSO
5 μM
15 μM
25 μM
WZ37
Medium
40
30
20
10
0
**
**
3 h
9 h
24 h
C
0 h
1 h
3 h
6 h
12 h
24 h
JC-1
D
DMSO
WZ37 3 h
WZ37 24 h
X20000
Mitochondria
Endoplasmic reticulum
E
Time (h) 0 1 3 6 12 24
DMSO
WZ37 Cur
5 15 25 25 (μM)
p-AKT
p-mTOR
BAD
PTEN
GAPDH

Figure 5

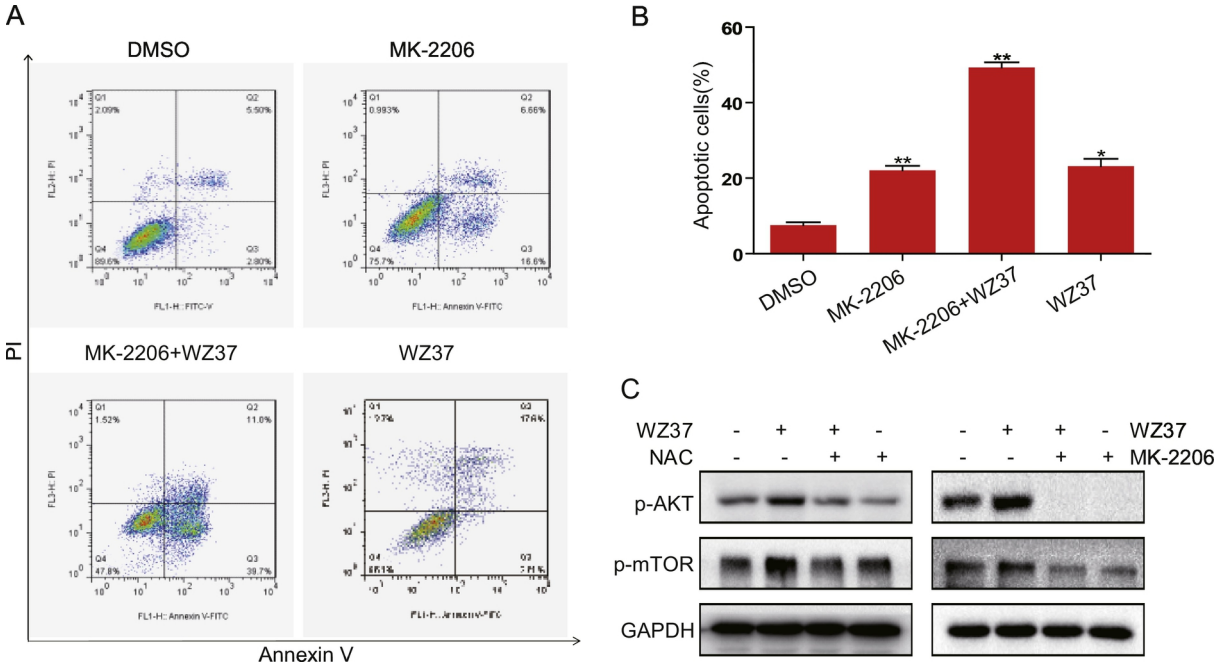
A
DMSO
MK-2206
MK-2206+WZ37
WZ37
PI
Annexin V
B
Apoptotic cells(%)
60
40
20
0
**
**
*
DMSO
MK-2206
MK-2206+WZ37
WZ37
C
WZ37 - + + - - + + - WZ37
NAC - - + + - - + + MK-2206
p-AKT
p-mTOR
GAPDH

Figure 6